Ab initio study of structural and magnetic properties of Si-doped Fe_2P

E. K. Delczeg-Czirjak,[1] L. Delczeg,[1] M. P. J. Punkkinen,[1,2] B. Johansson,[1,3] O. Eriksson,[3] and L. Vitos[1,3,4]
[1]*Applied Materials Physics, Department of Materials Science and Engineering, Royal Institute of Technology, SE-100 44 Stockholm, Sweden*
[2]*Department of Physics and Astronomy, University of Turku, FIN-20014 Turku, Finland*
[3]*Division for Materials Theory, Department of Physics and Materials Science, Uppsala University, SE-75121 Uppsala, Sweden*
[4]*Research Institute for Solid State Physics and Optics, H-1525 Budapest, P.O. Box 49, Hungary*
(Received 18 February 2010; revised manuscript received 30 June 2010; published 5 August 2010)

Ab initio electronic-structure methods are used to study the properties of $Fe_2P_{1-x}Si_x$ in ferromagnetic and paramagnetic states. The site preference and lattice relaxation are calculated with the projector augmented wave method as implemented in the Vienna *ab initio* simulation package. The paramagnetic state is modeled by the disordered local magnetic moment scheme, and the chemical and magnetic disorder is treated using the coherent potential approximation in combination with the exact muffin-tin orbital formalism. The calculated lattice parameters, atomic positions, and magnetic properties are in good agreement with the experimental and other theoretical results. In contrast to the observation, for the ferromagnetic state the body centered orthorhombic structure (bco, space group $Imm2$) is predicted to have lower energy than the hexagonal structure (hex, space group $P\bar{6}2m$). The zero-point spin fluctuation energy difference is found to be large enough to stabilize the hex phase. For the paramagnetic state, the hex structure is calculated to be the stable phase and the computed total energy versus composition indicates a hex to bco crystallographic phase transition with increasing Si content. The phonon vibrational free energy, estimated from the theoretical equation of state, turns out to stabilize the hexagonal phase, whereas the electronic and magnetic entropies favor the low symmetry orthorhombic structure.

DOI: 10.1103/PhysRevB.82.085103 PACS number(s): 71.15.Nc, 71.20.Gj, 64.30.Ef, 75.20.En

I. INTRODUCTION

Iron pnictides have attracted much attention in recent years due to their potential use in magnetic refrigeration. Several experimental works reported large magnetocaloric effect (MCE) near room temperature in MnFe(PAs)-based compounds.[1–7] Both the Curie temperature (T_C) and the MCE can be subtly tuned within the same crystal structure by substituting Fe and P/As. In other cases, substitution of Fe and P may lead to structural changes as well.[8,9]

The parent system for the above compounds is the hexagonal (hex) Fe_2P. In 1980s, Jernberg *et al.*[10] reported a phase transformation in Si-doped Fe_2P (Fig. 1). According to these measurements, the silicon atoms occupy the P sublattice and stabilize a body centered orthorhombic (bco) phase below a critical temperature (T_t). Around zero temperature, the system remains in the hex phase up to ~10% Si, and beyond this concentration the transition temperature shows a rapid increase with the Si amount. At temperatures larger than ~200 K, the structural transition occurs within a narrow temperature interval (~20 K).[10–12] Furthermore, the ferromagnetic (FM) transition temperature of $Fe_2P_{1-x}Si_x$ was found to increase from ~216 K for $x=0$ to ~660 K for $x=0.35$.[10] Since the composition dependence of T_C is weaker than that of T_t (Fig. 1), the two transition temperatures cross each other around $x \approx 0.28$ so that both crystallographic phases exist in the paramagnetic (PM) phase as well. It is interesting that the slope of the experimental T_t against Si content is almost constant for the two magnetic states and the slope of T_C is slightly reduced in the bco phase.

In spite of the comprehensive experimental data, the theoretical description of the effect of Si on the structural and magnetic properties of hexagonal Fe_2P and on the hex-bco phase transformation in $Fe_2P_{1-x}Si_x$ has remained scarce. In this work, we investigate the effect of Si doping on the structural and magnetic properties of ferromagnetic and paramagnetic Fe_2P and on the phase stability of paramagnetic Fe_2P. The structural and magnetic properties have been calculated using the *ab initio* exact muffin-tin orbital (EMTO)

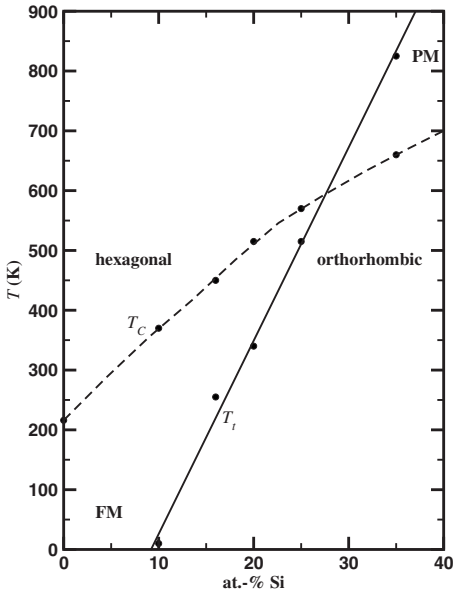

FIG. 1. Schematic phase diagram of the $Fe_2(PSi)$ system (Ref. 10). Shown are the hex-bco transition temperature T_t (solid line) and the Curie temperature T_C (dashed line) as a function of Si content.

method[13–17] and the projector augmented wave (PAW) method as implemented in the Vienna *ab initio* simulation package (VASP).[18–21] The paramagnetic state has been described within the disordered local magnetic moments (DLM) picture[22,23] and the chemical and magnetic disorder have been treated using the coherent potential approximation (CPA) (Refs. 24 and 25) in combination with the EMTO method.[16,17] For both crystallographic structures, the calculated lattice parameters, atomic positions, bulk moduli, and magnetic properties are in good agreement with the experimental and former theoretical values.[9,11,26–31] For the ferromagnetic state the bco structure is found to be the stable phase, in contrast to the experimental finding. At the same time, zero-point spin fluctuation energy is estimated to stabilize the ferromagnetic hex phase. Our first-principles approach qualitatively captures the observed hex-bco structural phase transitions in paramagnetic $Fe_2P_{1-x}Si_x$ although predicting a significantly larger two phase field than the one seen in experiments. Combining the present *ab initio* results with classical models for the thermal effects, we find that the magnetic and electronic entropy terms favor the paramagnetic bco phase, whereas the vibrational free energy strongly stabilizes the hex structure.

The rest of the paper is divided into three main sections and conclusions. Section II presents the theoretical tools. This includes a brief overview of the employed *ab initio* methods, the experimental crystal structures and the most important details of the numerical calculations. The *ab initio* results are presented and discussed in Sec. III. Here, we present the theoretical crystal structures and magnetic properties of Fe_2P, and investigate the effect of Si doping on the crystal structure, phase stability and magnetic properties of $Fe_2P_{1-x}Si_x$. In Sec. IV, we use classical models to interpret our findings from Sec. III. First, we compare the zero-point phonon and magnetic energies to the calculated energy difference between ferromagnetic hex and bco Fe_2P. Next, we investigate the chemical effect of Si and briefly discuss the temperature effects on the phase stability of paramagnetic $Fe_2P_{1-x}Si_x$.

II. THEORETICAL TOOLS

A. Total energy methods

We employed two different total energy methods to describe the thermophysical properties of $Fe_2P_{1-x}Si_x$ with $x \leq 0.4$. The exact muffin-tin orbital method[13–17] was used to treat the chemical and magnetic disorder, whereas the crystal structure relaxation was performed using projector augmented wave method.[18–21]

The EMTO theory formulates an efficient method for solving the Kohn-Sham equation.[32] It may be considered as an improved Korringa-Kohn-Rostoker method, where the exact Kohn-Sham potential is represented by large overlapping potential spheres. Inside these spheres the potential is spherically symmetric, and constant between the spheres. However, within the EMTO theory, in contrast to the usual muffin-tin based methods, the one-electron states are determined exactly (within the common numerical errors) for an optimized overlapping muffin-tin potential. This potential is chosen as the best possible spherical approximation to the exact potential:[14,17,33] the radii of the potential spheres, the spherical potential waves, and the constant value from the interstitial, are determined by minimizing (a) the deviation between the full potential and the overlapping muffin-tin potential and (b) the errors coming from the overlap between spheres. See Refs. 33 and 34 for further details about the potential optimization. In EMTO method, the substitutional disorder is treated using the coherent potential approximation[24,25] and the total energy is computed via the full charge-density technique.[35] The accuracy of the EMTO method for the equation of state of metals and disordered alloys has been demonstrated in a number of former works.[16,17,36–43]

The PAW method is a density-functional method using the plane-wave basis.[44,45] In PAW, the interaction between valence and core electrons is taken into account via pseudopotentials. For valence electrons, the Kohn-Sham equations are solved without shape approximation for the potential and density. It has been shown that PAW possesses the same accuracy as the full potential all electron methods.[46]

B. Crystal structure

The hexagonal phase of Fe_2P has the space group $P\bar{6}2m$ with six Fe atoms and three P atoms per unit cell. There are three Fe atoms of type Fe(I) and three of type Fe(II). Two phosphorus atoms have type P(I) and one type P(II). Fe(I) is surrounded by four P atoms which form a tetrahedron and Fe(II) by five P atoms forming a pyramid. Therefore Fe(I)-3*f* site is also called tetrahedral site and Fe(II)-3*g* pyramidal site.[47,48]

In early 1980s, Jernberg *et al.*[10] studied the crystal structure and magnetic properties of $Fe_2P_{1-x}Si_x$ with $x \leq 0.35$ using Mössbauer spectroscopy. According to them, Si addition to Fe_2P transforms the hex structure to a body centered orthorhombic structure with space group *Imm*2. In the orthorhombic structure, there are three different type of phosphorus sites P(1), P(2), and P(3), and six different type of iron sites Fe(1),Fe(2),…,Fe(6). The bco primitive cell contains four Fe(1), two Fe(2), two Fe(3), two Fe(4), one Fe(5), and one Fe(6) iron sites, and four P(1), one P(2), and one P(3) phosphorus sites.

In the following, for the description of the hex (bco) phase we use roman (Arabic) numbers. For reference, the experimental lattice parameters and atomic positions are given in parenthesis in Table I for hex Fe_2P (Ref. 49) and in Table II for bco $Fe_2P_{0.75}Si_{0.25}$.[11]

C. Details of the numerical calculations

The PAW method in combination with the local density approximation (LDA) (Ref. 50) and the Perdew-Burke-Ernzerhof (PBE) generalized gradient approximation[51] was used to determine the theoretical equilibrium crystal structure of hex and bco Fe_2P and $Fe_2P_{2/3}Si_{1/3}$ in the ferromagnetic state. In these calculations, the Fe 3*d* and 4*s*, and the P and Si 3*s* and 3*p* electrons were treated as valence electrons. The volume of the unit cell and the positions of the atoms

TABLE I. Theoretical (PAW-PBE) lattice parameters and atomic positions for hex Fe_2P. For reference, the experimental room-temperature values (Ref. 49) are shown in parenthesis.

		Space group: $P\bar{6}2m$		
		Lattice parameters		
		a=5.802(5.8675) Å	$b=a$	c=3.386(3.4581) Å
	Position	X	Y	Z
Fe(I)	3*f*	0.257 (0.25683)	0	0
Fe(II)	3*g*	0.591 (0.59461)	0	0.5
P(I)	2*c*	0.333	0.667	0
P(II)	1*b*	0	0	0.5

were relaxed using conjugate-gradient minimization of total energy until the remaining forces were less than 20 meV/Å. The number of k points in the irreducible wedge of the Brillouin zone was 324 and 100 for hex and bco structures, respectively. The k-point sampling was performed by the Monkhorst-Pack scheme.[52] The energy cutoff for plane waves was set to 500 eV. These values assured a convergence in the total energy of about 0.1 mRy.

The total energies of the $Fe_2P_{1-x}Si_x$ alloys were calculated using the EMTO method. The paramagnetic state was modeled by the disordered local magnetic moment approach.[22,23] This approximation accurately describes the paramagnetic state with randomly oriented local magnetic moments.[22] Here, we treated the $Fe_2P_{1-x}Si_x$ ternary system as a quaternary $(Fe^{\uparrow}_{0.5}Fe^{\downarrow}_{0.5})_2P_{1-x}Si_x$ alloy with a random mixture of two magnetic states of Fe. It has been shown that the total energy and the effective medium obtained with the DLM approach is suitable to calculate phase stability and magnetic properties of paramagnetic Fe alloys.[9,38,41,53,54] In the following, when referring to the theoretical PM state we mean the zero-temperature DLM state. The chemical disorder in the FM and PM states and the magnetic disorder in the PM state were treated using the CPA as implemented in the EMTO method.[16]

In the EMTO calculations, the one-electron equation was solved within the scalar-relativistic and soft-core approximations. The Green's function was calculated for 16 complex energy points distributed exponentially on a semicircular contour. In the basis set s,p and d orbitals were included, and in the one-center expansion of the full charge density l_{max}=8 cutoff was used. The electrostatic correction to the single-site coherent-potential approximation was described using the screened impurity model.[55] For Fe the 3*d* and 4*s* electrons and for P and Si the 3*s* and 3*p* electrons were treated as valence electrons. The Brillouin-zone sampling was performed using 45 and 175 uniformly distributed k points in the irreducible wedge of the hex and bco Brillouin zones, respectively. The self-consistent EMTO calculations were performed within LDA and the total energies were calculated using both LDA and PBE approximations.

Apart from some numerical errors, the PAW total energies are expected to represent the correct LDA or PBE level density-functional result. On the other hand, the EMTO method suffers from the shape approximation employed for the one-electron potential. In principle, the errors coming from this approximation can be lowered by increasing the number of basis functions included in the self-consistent calculation.[56] However, going beyond *spd* or *spdf* basis set is rather cumbersome in the case of large systems and therefore here we adopted a different approach. Full potential calculations have often been considered as reference for other electronic structure and total energy methods. Hence, here we used our PAW results obtained for the ferromagnetic Fe_2P as reference when minimizing the errors of the muffin-tin potential in the EMTO total energies. Finally, for the radii of the Fe, P, and Si potential spheres we arrived at $S_i=0.9\times w_i$, where w_i stands for the atomic radii of the Fe or P sites from the hex or bco structures.

TABLE II. Theoretical (PAW-PBE) lattice parameters and atomic positions for bco Fe_2P. For reference, the experimental room temperature values for $Fe_2P_{0.75}Si_{0.25}$ (Ref. 11) are shown in parenthesis.

		Space group: *Imm*2		
		Lattice parameters		
		a=6.502(6.533) Å	b=10.047(10.3632) Å	c=6.022(6.1425) Å
	Position	X	Y	Z
Fe(1)	8*e*	0.218 (0.219)	0.370 (0.373)	0.359 (0.372)
Fe(2)	4*c*	0.217 (0.217)	0	0.252 (0.251)
Fe(3)	4*d*	0	0.701 (0.701)	0.719 (0.725)
Fe(4)	4*d*	0	0.208 (0.208)	0.146 (0.152)
Fe(5)	2*b*	0	0.5	0.073 (0.083)
Fe(6)	2*a*	0	0	0.615 (0.607)
P,Si(1)	8*e*	0.269 (0.273)	0.334 (0.332)	0.990 (0.976)
P,Si(2)	2*b*	0	0.5	0.548 (0.517)
P,Si(3)	2*a*	0	0	0.968 (0.981)

TABLE III. Theoretical and experimental average Wigner-Seitz radii (w in units of Bohr) and bulk moduli (B in units of GPa) for hex and bco Fe_2P in the FM and PM states. The numbers in parentheses are the deviations (in %) relative to the average experimental values. The theoretical Wigner-Seitz radii were obtained using the EMTO and PAW method, and the theoretical bulk moduli using the EMTO method in combination with LDA and PBE.

			w_{hex}	w_{bco}	B_{hex}	B_{bco}
EMTO	FM	LDA	2.606 (−1.33)	2.596 (−2.07)	200.4	233.1
		PBE	2.664 (0.87)	2.656 (0.18)	186.8	195.4
	PM	PBE	2.660 (0.61)	2.657	160.9 (−5.07)	170.0
PAW	FM	LDA	2.543 (−3.71)	2.544 (−4.04)		
		PBE	2.618 (−0.87)	2.611 (−1.51)		
Expt.	FM		2.641[a]	2.651[b]		
	PM		2.644[c,d]		174[e],165[f]	

[a]Ferromagnetic, 85 K Ref. 48.
[b]Ferromagnetic, room temperature Ref. 11.
[c]Paramagnetic, room temperature Ref. 49.
[d]Paramagnetic, 285 K Ref. 48.
[e]Paramagnetic, room temperature Ref. 26.
[f]Paramagnetic, room temperature Ref. 27.

III. FIRST-PRINCIPLES RESULTS

A. Fe_2P

1. Theoretical crystal structure

In the structure optimization, we started from the experimental crystal structures and performed a full lattice relaxation within the corresponding space group using the PAW method and the PBE exchange-correlation approximation. The obtained theoretical lattice parameters and atomic positions for the ferromagnetic Fe_2P in the hex phase and in the hypothetical bco phase are listed in the Tables I and II. All further electronic structure and total energy calculations were performed using these theoretical data.

In the case of the hex structure (Table I), the theoretical internal coordinates agree very well with the experimental data. At the same time, it is found that PAW-PBE underestimates the a and c hexagonal lattice parameters of Fe_2P by 1.1% and 2.1%, respectively. For the bco structure, the deviation between the theoretical (Table II) and the experimental internal parameters are somewhat larger than for the hex structure. We ascribed this deviation to the fact that the experimental crystal structure was obtained for $Fe_2P_{0.75}Si_{0.25}$ whereas the present structural relaxation was done without Si. However, similar to the hex structure, PAW-PBE underestimates all three orthorhombic lattice parameters of Fe_2P compared to $Fe_2P_{0.75}Si_{0.25}$. Although Si slightly increases the equilibrium volume of Fe_2P (Sec. III B 1), the above underestimation cannot be accounted for by doping effect alone. It is more likely that the overbinding is connected with the accuracy of the exchange-correlation functionals.

In general, all recent gradient level exchange-correlation functionals yield accurate or slightly overestimated lattice parameters for metals.[57,58] Exceptions are the 3d metals, where the common approximations underestimate the equilibrium volume. The effect of the exchange-correlation approximation on the average Wigner-Seitz radius and bulk modulus of hex and bco Fe_2P is illustrated in Table III. In these tests, the crystal structures were fixed to the theoretical results from Tables I and II. The equilibrium properties were obtained from a Morse type of function[59] fitted to the theoretical total energies calculated for six different volumes. Results are shown for PAW and EMTO calculations. We find that for the equilibrium radius the large LDA errors are efficiently remedied by the PBE gradient correction. The EMTO method gives $w_{bco} \lesssim w_{hex}$, which is in a slight contrast with the experimental radii from Table III. This discrepancy may be ascribed to the effect of Si present in the experimental w_{bco}. The present theoretical bulk modulus for PM hex Fe_2P (161 GPa) is in good agreement with the average room-temperature experimental data of 169 GPa.[26,27] For comparison, for the bulk modulus of the nonmagnetic hex Fe_2P, using the PAW-PBE approach, Scott *et al.*[27] obtained 244 GPa at the theoretical volume and 175 GPa at the experimental volume. To our knowledge, no experimental bulk modulus is available for the bco phase.

2. Lattice stability of Fe_2P*-static conditions*

For the structural energy difference between the ferromagnetic bco and hex Fe_2P, viz. $\Delta E^{FM} \equiv E^{FM}_{bco} - E^{FM}_{hex}$, the PAW-PBE calculations give −0.124 mRy/atom. Using the LDA approach changes the structural energy difference to −0.024 mRy/atom. The main reason behind this difference is the small LDA equilibrium volume compared to PBE or experimental values (Table III). We note that an LDA calculation performed at the PBE volume (not shown) gives similar structural energy difference as the full PBE.

Based on the above figures, we conclude that at static conditions density-functional theory predicts the ferromagnetic bco structure as the stable phase. This finding is in disagreement with the experimental observation,[10] according to which Fe_2P adopts the hexagonal structure for temperatures down to 10 K. There are several possible reasons for

TABLE IV. Theoretical (EMTO-PBE) magnetic moments (μ_B) for FM and PM hex and bco Fe_2P. The paramagnetic phase is modeled using the DLM approach in combination with the EMTO method. The total ferromagnetic moments per formula unit (μ^{FM}) are given in the last row.

hex			bco		
Site	FM	PM	Site	FM	PM
Fe(I)	1.02	0	Fe(1)	1.38	0.25
			Fe(2)	1.00	0.00
Fe(II)	2.08	1.67	Fe(3)	1.72	1.54
			Fe(4)	2.21	1.96
			Fe(5)	2.31	2.23
			Fe(6)	1.02	0
P(I)	−0.10	0	P(1)	−0.11	0
P(II)	−0.08	0	P(2)	−0.10	0
			P(3)	−0.10	0
μ^{FM}	3.01	0		3.01	0

the above disagreement. First, we note that the resolving such small structural energy differences requires a very high numerical accuracy. We should also realize that a barely stable hexagonal phase would still disagree with the experimental phase diagram (Fig. 1). Namely, the fact that $Fe_2P_{1-x}Si_x$ remains in the hexagonal phase up to ~8% Si suggests that the correct energy difference between the two competing phases should be $\gtrsim$0.3 mRy/atom (see Sec. IV A). Combined with the present ΔE^{FM} values, this would mean that the error in our structural energy difference is around 0.3–0.4 mRy/atom. This is quite unlikely since PAW is commonly regarded as having the accuracy of the full potential all electron methods.[46] We recall that the error of the present PAW total energies is ~0.1 mRy/unit cell (i.e., $\lesssim$0.01 mRy/atom).

A possible explanation for the above disagreement between theory and experiment would be a complex noncollinear magnetic structure present in the hex phase at low temperatures as suggested by Mohn[60] and Kobayashi *et al.*[61] This is the topic of further investigations. Finally, we cannot rule out the possibility that the phonon or the spin quantum zero-point terms stabilize the hexagonal phase of ferromagnetic Fe_2P. These two effects may be estimated using classical models based on the calculated equation of state and density of state and will be discussed in details in Sec. IV A.

In order to establish the lattice stability for the paramagnetic Fe_2P we consider the DLM total energies. Using the EMTO-PBE approach, for the structural energy difference between the paramagnetic bco and hex Fe_2P, viz., $\Delta E^{PM} = E^{PM}_{bco} - E^{PM}_{hex}$, we obtain 0.865 mRy/atom (note that for the FM state the PAW and EMTO energy differences are the same). That is, within the disordered local magnetic moment picture the hexagonal structure is calculated to be the stable phase. This is in line with the experimental observation,[10] according to which paramagnetic Fe_2P has the hex crystal structure.

3. *Magnetic properties of* Fe_2P

The theoretical magnetic moments for ferromagnetic and paramagnetic Fe_2P are listed in Table IV. The magnetic moments on the P sites are due to the polarization effect of the Fe atoms and they are antiparallel to the Fe moments. Since for both structures the P moments are negligible, in the following we focus on the Fe moments only. In the case of the ferromagnetic hex structure, the magnetic moment for 3*g*-pyramidal Fe(II) site is 2.08 μ_B and that of the 3*f*-tetrahedral Fe(I) site is 1.02 μ_B. The total magnetic moment per formula unit μ^{FM}_{hex}=3.01 μ_B. These figures show a good agreement with the experimental[28–30] and former theoretical[9,11,31] data obtained for Fe_2P. For instance, Fujii *et al.*[48] measured 0.92 ± 0.02 μ_B and 1.70 ± 0.02 μ_B for the tetrahedral and pyramidal sites, respectively. The present magnetic moments are close to 0.89 μ_B on the 3*f* site and 1.81 μ_B on the 3*g* reported at 10 K for $(Fe_{0.93}Ni_{0.07})_2P$.[62]

For the ferromagnetic bco structure, there are six different Fe magnetic moments belonging to sites Fe(1),Fe(2),…,Fe(6). Sites Fe(1), Fe(2), and Fe(6) possess smaller magnetic moments compared to Fe(3), Fe(4), and Fe(5). The largest magnetic moment belongs to site Fe(5). The total bco magnetic moment per formula unit is very close to that in the hex phase, viz., $\mu^{FM}_{bco} \approx \mu^{FM}_{hex}$. Similar magnetic structure was obtained by Severin *et al.*[11] using the linear muffin-tin orbitals method. The small differences between the present magnetic moments and those reported in Ref. 11 can be ascribed to the employed methods as well as to the differences between the theoretical structures from Tables I and II and the experimental counterparts adopted in Ref. 11.

In the paramagnetic phase, modeled using the DLM approach, the net magnetic moment per formula unit is zero. We find that the local magnetic moments disappear on the 3*f*-tetrahedral site in the hex phase, on the Fe(2) and Fe(6) sites in the bco phase, and on all P sites. The local magnetic moments on the other sites have slightly lower values than in the ferromagnetic phase. Koumina *et al.*,[63] using neutron diffraction measurements, reported an abrupt decrease in the magnetic moments near the Curie temperature (T_C=217 K). At 230 K, for the magnetic moments they obtained ~0 μ_B for the 3*f*-tetrahedral site and ~0.6 μ_B for 3*g*-pyramidal site. This high temperature magnetic structure is well reflected by the present DLM results.

TABLE V. Theoretical (EMTO-PBE) hexagonal lattice parameters (in units of Å) for Fe_2P in the FM and PM states. For comparison, the PAW-PBE (Table III) and the experimental values are also listed.

	a	c	c/a
FM (EMTO)	5.927	3.467	0.585
FM (PAW)	5.802	3.386	0.584
FM (exp.)[a]	5.877	3.437	0.585
PM (EMTO)	5.844	3.553	0.608
PM (expt.)[b]	5.868	3.458	0.589
PM (expt.)[c]	5.868	3.458	0.589

[a]Ferromagnetic, 85 K Ref. 48.
[b]Paramagnetic, 285 K Ref. 48.
[c]Paramagnetic, room temperature Ref. 49.

4. Magnetostructural effect in hex Fe_2P

It is interesting to compare the theoretical lattice parameters calculated for the ferromagnetic and paramagnetic states of hex Fe_2P and relate them to the magnetoelastic effect reported by Fujii *et al.*[28] For this test we employ the EMTO method and the PBE approximation. The theoretical hexagonal lattice parameters for the FM and PM states of Fe_2P are listed in Table V, where, for comparison, we also included the PAW-PBE (Table I) values for the FM state and the experimental ones[48,49] for both states. In the EMTO structural relaxation, first we fixed the internal coordinates to the PAW-PBE values, then calculated the equilibrium volume for the fixed lattice and finally obtained the equilibrium c/a by computing the total energies for seven different c/a values by keeping the volume and internal positions constant. Taking into account these approximations, the agreement between EMTO and VASP, and between EMTO and experimental lattice parameters for the FM state may be considered to be reasonable.

In the next step, we repeated the EMTO calculations for the equilibrium lattice parameters of the PM state by employing the DLM approximation. Comparing the results obtained for the FM and PM states, we find that the theoretical equilibrium volume decreases by 0.5% when going from FM to PM. This change should be compared to the 0.9% exchange striction estimated by Fujii *et al.*[28] using Ni_2P as a prototype for the fictitious paramagnetic Fe_2P at 0 K.

We find that the theoretical lattice parameter a decreases by 0.083 Å, whereas c increases by 0.086 Å; upon magnetic disordering (Table V). The changes are much larger than the experimental discontinuities obtained at T_C.[28] However, since the present data contains no thermal effects, in order to be able to compare them to the experimental structural changes we need to extrapolate the experimental ferromagnetic and paramagnetic lattice parameters to 0 K. For the thermal expansion coefficients along the a (α_a) and c (α_c) axis we use the experimental ferromagnetic and paramagnetic values reported in Ref. 28. According to these, in the ferromagnetic phase $\alpha_a^{\mathrm{FM}}=-4.0\times10^{-5}$ 1/K and $\alpha_c^{\mathrm{FM}}=1.4\times10^{-5}$ 1/K, whereas the thermal expansion coefficients corresponding to the Curie-Weiss region (i.e., above ~500 K) are $\alpha_a^{\mathrm{PM}}=2.0\times10^{-5}$ 1/K and $\alpha_c^{\mathrm{PM}}\approx0$ 1/K. Starting from the measured lattice parameters[48] and assuming a linear temperature dependence, we find that when going from the FM to the PM state at 0 K, the experimental a decreases by 0.045 Å, and c increases by 0.025 Å. These estimations are in reasonable agreement with the present theoretical values.

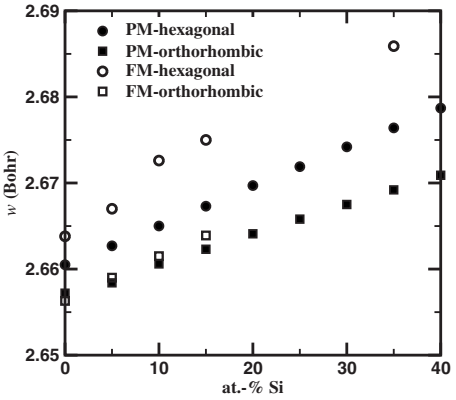

FIG. 2. The effect of Si doping on the equilibrium average Wigner-Seitz radius of ferromagnetic and paramagnetic hexagonal and orthorhombic $Fe_2P_{1-x}Si_x$. The paramagnetic phase is modeled using the DLM approach in combination with the EMTO method.

B. $Fe_2P_{1-x}Si_x$: The effect of Si doping

1. Equilibrium volume

The equilibrium average Wigner-Seitz radii of the hexagonal and orthorhombic $Fe_2P_{1-x}Si_x$ were computed using the EMTO-PBE method. Results are shown in Fig. 2 for both ferromagnetic and paramagnetic states. The theoretical average atomic radii exhibit an almost linear increase with x. For the FM state, the average concentration slopes (dw/dx) are 0.063 and 0.051 Bohr per atomic fraction (Bohr/a.f.) for the hex and bco structures, respectively. In the PM state, the increase in $w(x)$ with concentration is somewhat smaller: 0.046 Bohr/a.f. for hex and 0.035 Bohr/a.f. for bco. It is interesting that the large drop seen between the FM and PM volumes of the hex phase is not present in the bco phase. In fact, for $x=0$, $w_{\mathrm{bco}}^{\mathrm{FM}}$ is slightly smaller than $w_{\mathrm{bco}}^{\mathrm{PM}}$, whereas for $x>0.15$ we get the opposite trend.

To our knowledge, no direct experimental data is available for the effect of Si on the equilibrium volume of $Fe_2P_{1-x}Si_x$. Using the present concentration slope for the FM bco phase and the experimental equilibrium Wigner-Seitz radius of $Fe_2P_{0.75}Si_{0.25}$ (2.65 Bohr, Ref. 10), for the Wigner-Seitz radius of the Si-free bco structure we obtain $w_{\mathrm{bco}}=2.637$ Bohr. This extrapolated value is slightly smaller than the experimental Wigner-Seitz radius for the Si-free FM hex phase (2.64 Bohr, Ref. 49). We recall that within the PBE approximation both EMTO and PAW methods predict $w_{\mathrm{bco}}\lesssim w_{\mathrm{hex}}$ (Table III), in perfect agreement with the above estimate.

2. Site preference and lattice relaxation

The experimentally recorded Mössbauer spectra assumed a random distribution of Si on the P sites.[10] Because of that

TABLE VI. Total energies (mRy/atom) for the unrelaxed (E_u) and for the relaxed (E_r) hexagonal and orthorhombic $Fe_2P_{2/3}Si_{1/3}$. The position of the Si atom in the hexagonal cell is shown by P(I) and P(II), and the positions of the two Si atoms in the orthorhombic unit cell are shown by P(1), P(2), and P(3). P(1)* stands for the average of the three energies corresponding to the three different configurations obtained by placing two Si atoms on the 8*e* positions from the bco structure. For both structures the energies are given relative to the most stable position after relaxation.

Structure	Site	E_u	E_r
hex	P(I)	0.79	0.00
	P(II)	1.33	1.12
bco	P(1)	0.95	0.26
		1.01	0.41
		0.89	0.00
	P(1)*	0.95	0.22
	P(2),P(3)	3.36	2.81

the volume effects discussed in Sec. III B 1 were calculated by using randomly distributed Si atoms. However, since the individual volumes around different P sites in the hex (bco) phase differ by as much as 7.2% (9.6–11.7 %), a preferential site occupancy of the Si atoms on one of the P sites cannot be completely excluded. Recently, Liu and Altounian[64] reported a site preference for Si in hexagonal $MnFeP_{2/3}Si_{1/3}$. Their first-principles calculations carried out with the full potential-linear muffin-tin orbital method showed that Si prefers to occupy the 2*c* sites rather than 1*b* ones.

We investigated the effect of site preference for ferromagnetic $Fe_2P_{2/3}Si_{1/3}$ using the PAW-PBE method. We placed one Si atom on one of the P(I) or P(II) sites from the hexagonal unit cell and two Si atoms on P(1), P(2), or P(3) sites from the orthorhombic unit cell. The total energies obtained for the fixed underlying lattices (E_u) and for fully relaxed lattices (E_r) are shown in Table VI. For the prior case, we used the theoretical equilibrium lattices from Tables I and II and for the latter we performed full structural relaxation. For the bco phase, there are four equivalent P(1) sites, which become inequivalent after introducing two Si atoms per unit cell. The average energy of the resulting three different configurations is denoted by P(1)* in Table VI. We can see that the difference between different P(1) configurations is very small and thus in the following we consider only the average P(1)* energy.

In the hexagonal structure, the P(I) (2*c*) position turns out to be more preferable by 1.12 mRy/atom (0.54 mRy/atom for the unrelaxed structure) than the P(II) (1*b*) positions. For the orthorhombic structure, all P(1) (8*e*) configurations are more stable than the P(2) and P(3) sites and the average configuration is below the P(2) and P(3) sites by 2.59 mRy/atom (2.41 mRy/atom for the unrelaxed structure). For hex $Fe_2P_{2/3}Si_{1/3}$ the present result is in line with that reported by Liu *et al.*[64]

We note that the site preference for $Fe_2P_{2/3}Si_{1/3}$ is more pronounced for the bco structure than for the hex structure. It is highly unfavorable to put Si atoms on the P(2) or P(3) sites from the bco phase. This finding is consistent with the larger volume differences between different P sites in the bco phase compared to those in the hex phase and indicates that no reliable phase stability can be computed without considering the nonuniform distribution of Si atoms on P sites. The local lattice relaxation around the Si atoms keeps the site preference unchanged and gives similar relaxation energies for the two structures. For the stable site occupancy, the total energy is lowered with relaxation by $\sim$0.79 mRy/atom and $\sim$0.73 mRy/atom for the hex and bco lattices, respectively. Finally, we mention that taking into account the preferential site occupancy for the Si atoms has a small effect (well below 10%) on the theoretical volume versus composition slopes (Sec. I).

3. Magnetic properties

In Table VII, we compare the local magnetic moments for paramagnetic Fe_2P and $Fe_2P_{0.6}Si_{0.4}$. The magnetic structure corresponds to the equilibrium volume obtained by relaxing the volume but fixing the $b/a, c/a$ lattice parameters and the atomic coordinates to the theoretical values of Fe_2P (Tables I and II). For each composition, the Si atoms were distributed

TABLE VII. Theoretical (EMTO-PBE) local magnetic moments (μ_B) for paramagnetic hex and bco Fe_2P and $Fe_2P_{0.6}Si_{0.4}$. The paramagnetic phase is modeled using the DLM approach in combination with the EMTO method.

	hex			bco	
Site	Fe_2P	$Fe_2P_{0.6}Si_{0.4}$	Site	Fe_2P	$Fe_2P_{0.6}Si_{0.4}$
Fe(I)	0	0	Fe(1)	0.25	0.57
			Fe(2)	0.00	0.00
Fe(II)	1.67	1.78	Fe(3)	1.54	1.54
			Fe(4)	1.96	2.06
			Fe(5)	2.23	2.32
			Fe(6)	0.00	0.00
P(I)	0	0	P(1)	0	0
P(II)	0	0	P(2)	0	0
			P(3)	0	0

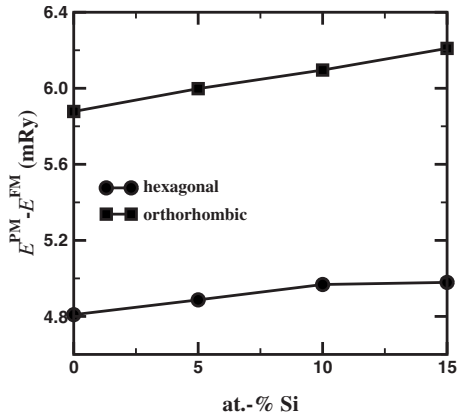

FIG. 3. Energy difference between the paramagnetic and the ferromagnetic phases of the hex and bco $Fe_2P_{1-x}Si_x$ as a function of Si content. The energies were calculated using the EMTO-PBE approach and the paramagnetic phase was modeled using the DLM approach.

on the P sites by taking into account the site preference.

We find that for both hex and bco phases, the theoretical PM moments slightly increase with Si doping. The average PM moment increases from 1.67 μ_B (1.71 μ_B) to 1.78 μ_B (1.97 μ_B) when 40% Si is introduced in hex (bco) Fe_2P. Notice that the difference between μ_{hex}^{PM} and μ_{bco}^{PM} increases with Si concentration.

The energy difference between the PM and FM phases $[\Delta E_{mag}(x)=E^{PM}(x)-E^{FM}(x)]$ of the hex and bco $Fe_2P_{1-x}Si_x$ is plotted in Fig. 3 as a function of x. In the simplest approximation, the magnetic energy can be related to the magnetic transition temperature. Thus, increasing $\Delta E_{mag}(x)$ with Si concentration suggests increasing $T_C(x)$, which is in accordance with the experiment.[10] On the other hand, the normalized slope of $\Delta E_{mag}(x)$ turns out to be significantly smaller than the normalized slope of $T_C(x)$. For instance, for the hexagonal phase we get $d\Delta E_{mag}(x)/dx/\Delta E_{mag}(0)\approx 0.33$ compared to $dT_C(x)/dx/T_C(0)\approx 5.69$.[10] Furthermore, the magnetic energy is about 20% larger for the bco than for the hex structure, suggesting somewhat larger transition temperature in the bco phase.

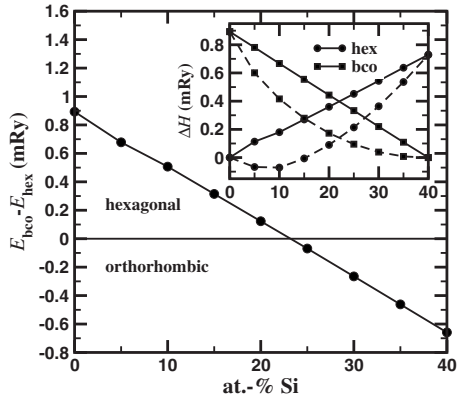

FIG. 4. Structural energy difference for paramagnetic $Fe_2P_{1-x}Si_x$ as a function of Si content. The paramagnetic phase was modeled using the DLM approach in combination with the EMTO method. Inset shows the mixing enthalpy (ΔH, solid lines) and ($\Delta H - T\Delta S_c$) for $T=700$ K (dashed lines, S_c being the configurational entropy) for hex and bco phases using as reference states the hexagonal phase for $x=0$ and the orthorhombic phase for $x=0.4$.

4. *Lattice stability of paramagnetic* $Fe_2P_{1-x}Si_x$*-static conditions*

Since for FM state theory predicts the bco structure to be the stable phase, it is beyond reason to discuss how the lattice stability is influenced by alloying for this magnetic state. Alternatively, one could focus on the PM state, for which the EMTO-PBE method in combination with the DLM approach predicts the hex structure to be the stable phase of Fe_2P and investigate how the structural energy difference $[\Delta E^{PM}(x) = E_{bco}^{PM}(x) - E_{hex}^{PM}(x)]$ varies with Si addition. The composition dependence of $\Delta E^{PM}(x)$ is shown in Fig. 4. The structural energy difference was computed from the volume relaxed total energies and taking into account the site preference but neglecting the local lattice relaxations (i.e., using rigid lattices).

We find that for paramagnetic $Fe_2P_{1-x}Si_x$, the hex total energy remains below the bco total energy up to ~23% Si. According to that, at static condition the stability field of the hex phase is located below and that of the bco phase above $x\approx 0.23$. This is consistent with the experimental result.[10,12] On the other hand, using the common tangent technique, we find that at low temperature the present theory predicts a wide two phase field between the hex and bco phases (Fig. 4, inset, solid lines), compared to the negligible miscibility gap found in experiment.[10] According to Jernberg and coworkers, in $Fe_2P_{1-x}Si_x$ the structural transformation takes place within ~20 K, which corresponds to ~1% Si wide two phase field as estimated from Fig. 1. We note that in Ref. 12 the width of the two phase field was estimated to be somewhat larger (~7% Si). Although the temperature dependent terms in the free energy (e.g., the configurational entropy) reduce the width of the theoretical miscibility gap, the above contradiction cannot be explained merely by thermal effects (Sec. IV C).

IV. DISCUSSION

In the previous section, we presented the structural and magnetic properties calculated from first-principles theory for ferromagnetic and paramagnetic Fe_2P and $Fe_2P_{1-x}Si_x$. In the following, first we estimate the zero-point phonon and magnetic energy contribution to the phase stability of ferromagnetic Fe_2P. Next, we discuss the electronic structure origin of the effect of Si on the structural energy difference and briefly comment on the possible thermal effects on the phase stability of paramagnetic $Fe_2P_{1-x}Si_x$.

A. Zero-point energies

In contrast to the observation, theory (PAW-PBE) predicts that the ferromagnetic bco structure has by $|\Delta E^{FM}| = 0.124$ mRy/atom lower total energy than that of the hex structure (Sec. III A 2). A plausible explanation for the above disagreement would be the zero-point phonon vibration term (ΔE_{ph}^{zp}). Using the expression

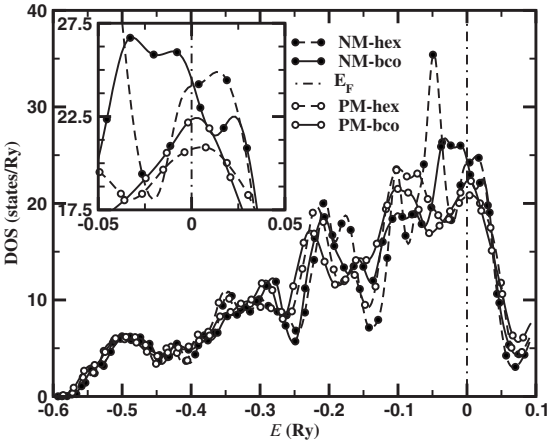

FIG. 5. Average density of states for hex (dashed line) and bco (solid line) Fe_2P. The energies are relative to the Fermi level (E_F). Solid symbols are for nonmagnetic and open symbols for paramagnetic states. Inset shows the DOS around the Fermi level.

$$\Delta E_{\rm ph}^{\rm zp} \approx \frac{9}{8} k_{\rm B} (\Theta_{\rm D}^{\rm bco} - \Theta_{\rm D}^{\rm hex}) \tag{1}$$

($k_{\rm B}$ is the Boltzmann constant) a difference of $\Delta\Theta_{\rm D} = \Theta_{\rm D}^{\rm bco} - \Theta_{\rm D}^{\rm hex} \approx 18$ K between the bco and hex Debye temperatures would be enough to overcome the calculated total energy difference between the two ferromagnetic structures. The Debye temperature may be estimated from the bulk parameters as

$$\Theta_{\rm D} = \frac{h}{k_{\rm B}} \left(\frac{4\pi}{3} \right)^{-1/6} F(\nu) \left(\frac{wB}{M} \right)^{1/2}, \tag{2}$$

where h is the Planck constant, ν the Poisson ratio (here we assume $\nu_{\rm hex} = \nu_{\rm bco} = 0.33$), M average atomic mass, w the Wigner-Seitz radius, and B the bulk modulus. The function $F(\nu)$ is defined in Ref. 65. Equation (2) in combination with the calculated bulk parameters from Table III yields $\Delta\Theta_{\rm D} \approx 12$ K, which is below the minimum value of 18 K needed to stabilize the hex phase.

On the other hand, close to zero temperature, the Si-doped system remains in the hexagonal phase up to ~8% Si.[10] Using the mixing enthalpy versus composition slope calculated for the ferromagnetic structures (not shown), we find that in Si-free system the total energy of the hex phase should be by ~0.27 mRy below that of the bco phase. This energy difference combined with the present $\Delta E^{\rm FM}$ would require $\Delta E_{\rm ph}^{\rm zp} \approx 0.394$ mRy or $\Delta\Theta_{\rm D} \approx 54$ K, which represents about 13% of the experimental Debye temperature of FM Fe_2P (420 K, Ref. 66). This is an unusually large difference between the Debye temperatures of systems with similar chemical bonding,[67] making it unlikely that the zero-point phonon term by itself is responsible for the stability of the hex phase. We should also mention, however, that very large $\Delta\Theta_{\rm D}/\Theta_{\rm D}$ may arise if one of the competing structures (in our case the hex structure) is barely stable dynamically.[39]

In magnetic materials, the zero-point spin fluctuation term should also be considered when calculating the lattice stability at 0 K. For both crystal structures, there is a peak in the density of states (DOS) near the Fermi level (E_F) (Fig. 5) indicating that Fe_2P is a weak ferromagnet. Namely, for the hex phase the nonmagnetic (NM) DOS is $N(E_F) = 24.1$ states/Ry compared to 20.8 states/Ry obtained for the PM state. The above figures for the bco phase are 24.5 states/Ry and 22.3 states/Ry for the NM and PM states. Within the Stoner model, the magnetic susceptibility of a weak ferromagnet is given by[68]

$$\chi = \frac{3\mu_{\rm B}^2 N(E_F)}{\zeta^2 c}, \tag{3}$$

where $\zeta = (n^{\uparrow} - n^{\downarrow})/n$ is the relative magnetization ($n = n^{\uparrow} + n^{\downarrow}$, $n^{\uparrow}$ and $n^{\downarrow}$ being the spin occupation numbers) and

$$c = -\frac{1}{8} \frac{n^2}{N(E_F)^2} \left\{ \frac{N(E_F)''}{N(E_F)} - 3 \left[\frac{N(E_F)'}{N(E_F)} \right]^2 \right\}, \tag{4}$$

where $'$ and $''$ stand for first- and second-order energy derivatives, respectively. From the self-consistent DOS of NM Fe_2P, we have $N(E_F)_{\rm bco} \approx N(E_F)_{\rm hex}$, $N(E_F)'_{\rm bco} \approx -8.1 \times N(E_F)'_{\rm hex}$, and $N(E_F)''_{\rm bco} \approx 1.2 \times N(E_F)''_{\rm hex}$, yielding $\chi_{\rm hex} \approx 1.8 \chi_{\rm bco}$. Since χ^{-1} gives the second order derivative of the magnetic energy near the equilibrium magnetic moment, we obtain that the hexagonal structure is magnetically softer than the bco structure. Accordingly, the zero-point spin fluctuations[69–72] are expected to stabilize the hex phase relative to the bco phase.

In order to estimate the zero-point spin fluctuation energy contribution to the structural energy difference ($\Delta E_{\rm SF}^{\rm zp}$) we employ the expression proposed by Solontsov *et al.*[70,72]

$$E_{\rm SF}^{\rm zp} \approx \frac{3}{4\pi} \hbar \omega_{\rm SF} \ln \frac{\omega_{\rm SF}^2 + \omega_c^2}{\omega_{\rm SF}^2}, \tag{5}$$

where $\hbar = h/2\pi$. The characteristic frequency of the spin fluctuation $\omega_{\rm SF}$ is obtained from the magnetic susceptibility χ and the magnetic relaxation rate $\Gamma(\omega_{\rm SF} = \Gamma\chi)$, and the cutoff frequency ω_c is taken from experiments.[71] For the present purpose, we use the approximations $\hbar\omega_{\rm SF} \sim \chi^{-1}\mu_{\rm B}^2$ and $\hbar\omega_c \gg k_{\rm B} T_{\rm melt}$.[72] Taking the lower limit for the cutoff frequency $\omega_c = \omega_c^{\rm min}$ ($\omega_c^{\rm min} \equiv k_{\rm B} T_{\rm melt}/\hbar$ with $T_{\rm melt}$ from Ref. 73) gives $\Delta E_{\rm SF}^{\rm zp} \approx 0.3$ mRy/atom, whereas $\omega_c = 2\omega_c^{\rm min}$ results in $\Delta E_{\rm SF}^{\rm zp} \approx 0.5$ mRy/atom. That is, the zero-point quantum spin fluctuation term could indeed stabilize the hexagonal phase of Fe_2P at low temperature. For a final conclusion, however, more accurate values for the characteristic frequencies and cut-off frequencies are needed.

B. Chemical effect of Si

The structural change from Fig. 4 has mainly chemical origin and can be understood by monitoring the total energy components of paramagnetic $Fe_2P_{1-x}Si_x$ alloys. According to the simple picture of the metallic bonds,[74] the crystal structure is determined by the balance of the Madelung and the Peierls terms. The prior gives the electrostatic energy and the latter is connected to the change in the one-electron energy upon lattice distortion. More generally, the Peierls term includes all electronic structure changes (not necessarily symmetry lowering deformations) that lead to the decrease of the kinetic energy.

Within a simple approximation,[75] the Madelung term is proportional to $(1.8-\alpha^{M})$, where α^{M} is the Madelung constant of the lattice. Accordingly, when α^{M} decreases the electrostatic energy increases. In our case, $\alpha^{M}_{hex}=1.7720$ and $\alpha^{M}_{bco}=1.7739$. Hence, the average electrostatic energy of Fe_2P should be slightly smaller in the bco phase than in the hex phase. In other words, the Madelung term favors the bco phase. Indeed, the total electrostatic energy for the paramagnetic hex Fe_2P is −3779.227270 Ry/atom compared to −3779.243642 Ry/atom obtained for the paramagnetic bco phase. On the other hand, we find that the kinetic energy (plus the exchange-correlation term) is smaller for the hex phase (1854.099890 Ry/atom) than for the bco phase (1854.117127 Ry/atom). The difference between the kinetic (one-electron) energies is also reflected in the total density of states for the hex and bco structure (Fig. 5, open symbols). In particular, the DOS at the Fermi level is smaller for the hex phase than for the bco phase.

Silicon doping changes the bonding in such a way that the kinetic (plus exchange-correlation) energy decreases, i.e., both structures become more stable kinetically. This effect is more pronounced for the hex structure than for the bco structure, which is represented in increasing kinetic-energy difference from 17.238 mRy/atom to 18.401 mRy/atom upon 40% Si addition. The electrostatic energy shows the opposite trend: for both structures the electrostatic energy increases with Si doping. This is in line with the observation that the average interstitial charge density decreases by 0.002273 electron/a.u.^{3} for the hex structure and by 0.001836 electron/a.u.^{3} for the bco structure when 40% Si is added to Fe_2P (note that Si has less number of electrons than P). Since the above change is more pronounced for the hex structure, the difference between the bco and hex electrostatic energies changes from −16.373 mRy/atom corresponding to Fe_2P to −19.123 mRy/atom obtained for $Fe_2P_{0.6}Si_{0.4}$. Hence, the electrostatic destabilization effect of Si is larger in the hex structure than in the bco structure, which together with the kinetic energy change leads to the stabilization of the bco phase against the hex phase with Si addition.

C. Temperature effects

In this section, we briefly discuss the effect of temperature on the phase stability of paramagnetic $Fe_2P_{1-x}Si_x$. Since no accurate phonon spectra was established, these results are mainly intended to give a qualitative estimate how the temperature affects the stability field of the hexagonal and orthorhombic phases.

Before turning to the phonon contribution and to the electronic and magnetic entropy terms, we first briefly discuss the effect of the mixing entropy. The configurational entropy (S_c), calculated within the mean-field approximation, has no effect on the structural free energy difference ($F^{bco}-F^{hex}$) but slightly reduces the width of the two phase field. As an example, in inset of Fig. 4 we show the mixing enthalpy minus $T\Delta S_c$ for hex and bco phases at $T=700$ K. We find that at this temperature, the configurational term increases the stability range of the hexagonal $Fe_2P_{1-x}Si_x$ from $x=0$ to $x \approx 0.10$. However, the miscibility gap between the hex and bco phases still remains large, in disagreement with the observation.[10] Assuming that the present mixing enthalpies from the inset of Fig. 4 represent the correct density functional result for $Fe_2P_{1-x}Si_x$, it is clear that further thermal effects are needed to resolve the above discrepancy between theory and experiment.

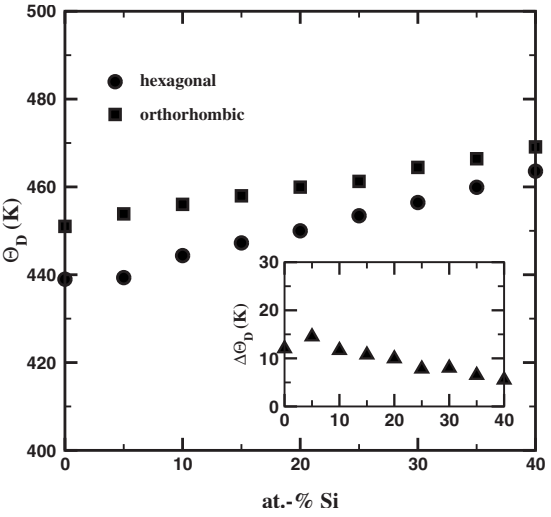

FIG. 6. Theoretical (EMTO-PBE) Debye temperatures of paramagnetic hex and bco $Fe_2P_{1-x}Si_x$ plotted as a function of Si content. In inset, the Debye temperature difference $\Delta\Theta_D=\Theta_D^{bco}-\Theta_D^{hex}$ is shown.

The phonon free energy may be estimated using the Debye model with the characteristic temperature given in Eq. (2). In general, smaller Debye temperature corresponds to softer lattice and to larger vibrational terms in the free energy.[67] For paramagnetic $Fe_2P_{1-x}Si_x$ with $0 \le x \le 0.4$, we have $w^{PM}_{bco} < w^{PM}_{hex}$ (Fig. 2). The calculated bulk modulus of the hex (bco) phase, on the other hand, increases from 161 GPa (170 GPa) to 175 GPa (181 GPa) as the Si content increases from zero to 40%. Hence, the trend of the bulk modulus turns out to be the dominant term in the Debye temperature, yielding $\Theta_D^{hex} < \Theta_D^{bco}$ for all x values considered here (Fig. 6). That is, the phonon vibration stabilizes the hexagonal structure against the orthorhombic structure. This stabilization effect is in fact responsible for the broadening of the stability field of the hexagonal phase with increasing T (Fig. 1). On the other hand, the difference between Θ_D^{hex} and Θ_D^{bco} decreases with Si addition (Fig. 6, inset), which means that the phonon contribution to the stability of hex $Fe_2P_{1-x}Si_x$ reduces with x.

For a quantitative estimate of the phonon free energy, we make use of the high-temperature expansion of the phonon free energy.[76,77] According to that the phonon vibration contribution to the bco-hex free energy difference may be approximated as

$$\Delta F_{ph}(T) \approx 3k_B T \frac{\Theta_D^{bco}-\Theta_D^{hex}}{\Theta_D^{bco}}. \quad (6)$$

The present results for $\Delta F_{ph}(T)$ are listed in Table VII for $x=0$ and $x=0.4$ at $T=700$, 800, and 900 K. Compared to the

TABLE VIII. Phonon vibration (ΔF_{ph}), electronic entropy (ΔF_e), and magnetic entropy (ΔF_m) contributions to the free-energy difference between the paramagnetic hex and bco $Fe_2P_{1-x}Si_x$. Energies are listed in mRy/atom for $x=0$ and $x=0.4$, and for temperatures $T=700$, 800, and 900 K.

	ΔF_{ph}		ΔF_e		ΔF_m	
T	Fe_2P	$Fe_2P_{0.6}Si_{0.4}$	Fe_2P	$Fe_2P_{0.6}Si_{0.4}$	Fe_2P	$Fe_2P_{0.6}Si_{0.4}$
700	0.35	0.16	−0.11	−0.05	−0.06	−0.24
800	0.41	0.18	−0.14	−0.07	−0.06	−0.28
900	0.46	0.20	−0.18	−0.08	−0.07	−0.31

internal energy difference from Fig. 4, the present $\Delta F_{ph}(T)$ values turn out to be rather significant. For example, by including $\Delta F_{ph}(700\ \mathrm{K})$ in the free energy difference between the bco and hex phases shifts the concentration, where $(F^{bco}-F^{hex})$ crosses zero from $x\approx 0.23$ (Fig. 4) to $x\gtrsim 0.3$. The above estimate clearly demonstrates that no accurate phase stability study of $Fe_2P_{1-x}Si_x$ can be performed without properly accounting for the phonon contributions to the free energies of the hex and bco phases.

Going beyond the above simple Debye model requires the determination of the phonon spectra for the hex and bco structures as a function of Si concentration. This is an enormous task, especially for the paramagnetic phase and it is beyond the reach of the present *ab initio* tools. Based on the present results for the free energy differences obtained for rigid lattices, we suggest that the experimentally observed unusually narrow transition zone between the hex and bco phases is due to the soft modes in the phonon spectrum of the hexagonal structure. Note that soft phonon modes would also support the idea that the hex phase of Fe_2P is barely stable (Sec. IV A).

The electronic entropy may be calculated using the approximation[67] $S^e\approx\frac{2\pi^2}{3}N(E_F)k_B^2T$, and the corresponding contribution $\Delta F_e=-T(S^e_{bco}-S^e_{hex})$ to the free energy difference between the bco and hex phases is given in Table VII for $x=0$ and $x=0.4$ and for temperatures $T=700$, 800, and 900 K. We find that the electronic entropy has a bco stabilizing effect in Fe_2P, which is slightly diminished with Si addition.

The effect of the magnetic entropy in the PM state may be estimated using the mean-field approximation $S^m=k_B\Sigma_i\ln(\mu_i+1)$ (μ_i is the magnetic moment for site i) valid for a completely disordered magnetic state.[76] The magnetic free energy term $\Delta F_m=-T(S^m_{bco}-S^m_{hex})$ calculated using the moments from Table VII, is shown in Table VIII for $x=0$ and $x=0.4$ and $T=700$, 800, and 900 K. Since the DLM moments are somewhat larger for the bco structure than for the hex structure, the magnetic entropy always stabilizes the bco phase. The effect is small (below −0.1 mRy/atom) for Fe_2P but increases significantly with Si addition.

Summing up the phonon vibration, the electronic and magnetic entropy terms, we find that in paramagnetic Fe_2P the thermal effects stabilize the hex phase by ~0.18 mRy/atom at 700 K and by ~0.21 mRy/atom at 900 K. However, this effect is gradually diminished with Si addition and changes sign around 20–25 % Si and $T\gtrsim 700$ K (i.e., still within the stability field of the hex phase). When 40% Si is added, the total thermal effect favors the bco phase by −0.13 mRy/atom at 700 K and −0.19 mRy/atom at 900 K.

V. CONCLUSIONS

Using the EMTO and PAW methods, we have investigated the bulk properties of hexagonal and orthorhombic $Fe_2P_{1-x}Si_x$ as a function of Si content. For Si free systems, the present theoretical hexagonal and orthorhombic crystal structures are in good agreement with the former experimental data. We find that the shape and the volume of the hexagonal unit cell changes upon ferromagnetic-paramagnetic transition, in good agreement with the experiments. In the ferromagnetic state, theory predicts the bco structure to be slightly more stable than the experimentally observed hex structure. We ascribe this discrepancy either to a barely stable hex structure (with soft phonon modes) or to zero-point quantum spin fluctuations. In the paramagnetic state, modeled using the DLM picture, the hexagonal structure is calculated to be the stable phase, in line with the observations.

Silicon addition increases the equilibrium volume of Fe_2P in an almost linear manner. We find that in the ferromagnetic state, the Si atoms prefer the P(I) site from the hex structure and the P(1) site from the bco structure. The Si site preference turns out to be significant for both structures, contradicting to the uniform site distribution assumed in experiments. The calculated magnetic moments for both magnetic states are in good agreement with the experimental and former theoretical values. The energy difference between the ferromagnetic and paramagnetic (DLM) state increases with Si, indicating increasing transition temperature within both crystallographic phases.

The experimentally observed hex-bco crystallographic phase transition is reproduced by the theoretical calculations performed for the paramagnetic state. However, in contrast to the observations, the present theoretical phase transition occurs through a wide two phase field. This deviation might be due to the softening of the hexagonal lattice with Si addition, not accounted for by the present calculations. Using simple models, we have estimated the thermal effects on the phase stability. Phonon vibrations are found to favor the hexagonal structure, whereas the electronic and magnetic entropy stabilize the bco phase. The total thermal effect changes sign around 20–25 % Si. The present theoretical results and the slight disagreement between the theoretical

and experimental properties of $Fe_2P_{1-x}Si_x$ call for further more accurate experimental as well as theoretical investigations.

ACKNOWLEDGMENTS

Discussions with Yvonne Andersson are greatly acknowledged. The Swedish Research Council, the Swedish Foundation for Strategic Research, the Carl Tryggers Foundation, and the Swedish Energy Agency are acknowledged for financial support. Parts of the calculations were performed on UPPMAX resources. The computer resources of the Finnish IT Center for Science (CSC) and Mgrid project are also acknowledged.

[1] E. Brück, O. Tegus, L. Zhang, X. W. Li, F. R. de Boer, and K. H. J. Buschow, J. Alloys Compd. **383**, 32 (2004).
[2] E. Brück, J. Phys. D **38**, R381 (2005).
[3] E. Brück, O. Tegus, D. T. Cam Thanh, and K. H. J. Buschow, J. Magn. Magn. Mater. **310**, 2793 (2007).
[4] E. Brück, M. Ilyn, A. M. Tishin, and O. Tegus, J. Magn. Magn. Mater. **290-291**, 8 (2005).
[5] W. Dagula, O. Tegus, X. W. Li, L. Song, E. Brück, D. T. Cam Thanh, F. R. de Boer, and K. H. J. Buschow, J. Appl. Phys. **99**, 08Q105 (2006).
[6] O. Tegus, E. Brück, X. W. Li, L. Zhang, W. Dagula, F. R. de Boer, and K. H. J. Buschow, J. Magn. Magn. Mater. **272-276**, 2389 (2004).
[7] D. Fruchart, F. Allab, M. Balli, D. Gignoux, E. K. Hlil, A. Koumina, N. Skryabina, J. Tobola, P. Wolfers, and R. Zach, Physica A **358**, 123 (2005).
[8] D. T. Cam Thanh, E. Brück, N. T. Trung, J. C. P. Klaasse, K. H. J. Buschow, Z. Q. Ou, O Tegus, and L. Caron, J. Appl. Phys. **103**, 07B318 (2008).
[9] B. Wiendlocha, J. Tobola, S. Kaprzyk, R. Zach, E. K. Hlil, and D. Fruchart, J. Phys. D **41**, 205007 (2008).
[10] P. Jernberg, A. A. Yousif, L. Häggström, and Y. Andersson, J. Solid State Chem. **53**, 313 (1984).
[11] L. Severin, L. Häggström, L. Nordström, Y. Andersson, and B. Johansson, J. Phys.: Condens. Matter **7**, 185 (1995); O. Eriksson, J. Sjöström, B. Johansson, L. Häggström, and H. L. Skriver, J. Magn. Magn. Mater. **74**, 347 (1988).
[12] D. Lindell, Ph.D. thesis, Uppsala University, 2007.
[13] O. K. Andersen, O. Jepsen, and G. Krier, *Lectures on Methods of Electronic Structure Calculation* (World Scientific, Singapore, 1994), p. 63.
[14] L. Vitos, H. L. Skriver, B. Johansson, and J. Kollár, Comput. Mater. Sci. **18**, 24 (2000).
[15] L. Vitos, Phys. Rev. B **64**, 014107 (2001).
[16] L. Vitos, I. A. Abrikosov, and B. Johansson, Phys. Rev. Lett. **87**, 156401 (2001).
[17] L. Vitos, *Computational Quantum Mechanics for Materials Engineers* (Springer-Verlag, London, 2007).
[18] G. Kresse and J. Hafner, Phys. Rev. B **47**, 558 (1993).
[19] G. Kresse and J. Hafner, Phys. Rev. B **49**, 14251 (1994).
[20] G. Kresse and J. Furthmüller, Comput. Mater. Sci. **6**, 15 (1996).
[21] G. Kresse and J. Furthmüller, Phys. Rev. B **54**, 11169 (1996).
[22] A. J. Pindor, J. Stauton, G. M. Stocks, and H. Winter, J. Phys. F: Met. Phys. **13**, 979 (1983).
[23] B. L. Gyorffy, A. J. Pindor, J. Stauton, G. M. Stocks, and H. Winter, J. Phys. F: Met. Phys. **15**, 1337 (1985).
[24] P. Soven, Phys. Rev. **156**, 809 (1967).
[25] B. L. Gyorffy, Phys. Rev. B **5**, 2382 (1972).
[26] P. Dera, B. Lavina, L. A. Borkowski, V. B. Prakapenka, S. R. Sutton, M. L. Rivers, R. T. Downs, N. Z. Boctor, and Ch. T. Prewitt, Geophys. Res. Lett. **35**, L10301 (2008).
[27] H. P. Scott, B. Kiefer, C. D. Martin, N. Boateng, M. R. Frank, and Y. Meng, High Press. Res. **28**, 375 (2008).
[28] H. Fujii, T. Hōkabe, T. Kamigaichi, and T. Okamato, J. Phys. Soc. Jpn. **43**, 41 (1977).
[29] O. Beckman and L. Lundgren, in *Handbook of Magnetic Materials*, edited by K. H. J. Buschow (Elsevier Science, Amsterdam, 1991), Vol. 6, p. 231.
[30] R. Wäppling, L. Häggström, T. Ericsson, S. Devanarayanan, E. Karlsson, B. Carlsson, and S. Rundqvist, J. Solid State Chem. **13**, 258 (1975).
[31] J. B. Goodenough, J. Solid State Chem. **7**, 428 (1973).
[32] W. Kohn and L. J. Sham, Phys. Rev. **140**, A1133 (1965).
[33] O. K. Andersen, C. Arcangeli, R. W. Tank, T. Saha-Dasgupta, G. Krier, O. Jepsen, and I. Dasgupta, Mater. Res. Soc. Symp. Proc. **491**, 3 (1998).
[34] M. Zwierzycki and O. K. Andersen, Acta Phys. Pol. A **115**, 64 (2009).
[35] J. Kollár, L. Vitos, and H. L. Skriver, in *Electronic Structure and Physical Properties of Solids: The Uses of the LMTO method*, Lectures Notes in Physics, edited by H. Dreyssé (Springer-Verlag, Berlin, 2000), p. 85.
[36] A. Taga, L. Vitos, B. Johansson, and G. Grimvall, Phys. Rev. B **71**, 014201 (2005).
[37] Z. Nabi, L. Vitos, B. Johansson, and R. Ahuja, Phys. Rev. B **72**, 172102 (2005).
[38] L. Vitos, P. A. Korzhavyi, and B. Johansson, Nature Mater. **2**, 25 (2003).
[39] B. Magyari-Köpe, G. Grimvall, and L. Vitos, Phys. Rev. B **66**, 064210 (2002); **66**, 179902(E) (2002).
[40] B. Magyari-Köpe, L. Vitos, and G. Grimvall, Phys. Rev. B **70**, 052102 (2004).
[41] L. Vitos, P. A. Korzhavyi, and B. Johansson, Phys. Rev. Lett. **88**, 155501 (2002).
[42] L. Huang, L. Vitos, S. K. Kwon, B. Johansson, and R. Ahuja, Phys. Rev. B **73**, 104203 (2006).
[43] A. E. Kissavos, S. I. Simak, P. Olsson, L. Vitos, and I. A. Abrikosov, Comput. Mater. Sci. **35**, 1 (2006).
[44] P. E. Blöchl, Phys. Rev. B **50**, 17953 (1994).
[45] G. Kresse and D. Joubert, Phys. Rev. B **59**, 1758 (1999).
[46] A. Kiejna, G. Kresse, J. Rogal, A. De Sarkar, K. Reuter, and M. Scheffler, Phys. Rev. B **73**, 035404 (2006).
[47] D. Scheerlinck and E. Legrand, Solid State Commun. **25**, 181 (1978).
[48] H. Fujii, S. Komura, T. Takeda, T. Okamoto, Y. Ito, and J. Akamitsu, J. Phys. Soc. Jpn. **46**, 1616 (1979).

[49] B. Carlsson, M. Gölin, and S. Rundqvist, J. Solid State Chem. **8**, 57 (1973).
[50] J. P. Perdew and Y. Wang, Phys. Rev. B **45**, 13244 (1992).
[51] J. P. Perdew, K. Burke, and M. Ernzerhof, Phys. Rev. Lett. **77**, 3865 (1996).
[52] H. J. Monkhorst and J. D. Pack, Phys. Rev. B **13**, 5188 (1976).
[53] L. Vitos, P. A. Korzhavyi, and B. Johansson, Phys. Rev. Lett. **96**, 117210 (2006).
[54] H. Pitkänen, M. Alatalo, A. Puisto, M. Ropo, K. Kokko, M. P. J. Punkkinen, P. Olsson, B. Johansson, S. Hertzman, and L. Vitos, Phys. Rev. B **79**, 024108 (2009).
[55] P. A. Korzhavyi, A. V. Ruban, I. A. Abrikosov, and H. L. Skriver, Phys. Rev. B **51**, 5773 (1995).
[56] N. I. Al-Zoubi, M. P. J. Punkkinen, B. Johansson, and L. Vitos, Phys. Rev. B **81**, 045122 (2010).
[57] M. Ropo, K. Kokko, and L. Vitos, Phys. Rev. B **77**, 195445 (2008).
[58] G. I. Csonka, J. P. Perdew, A. Ruzsinszky, P. H. T. Philipsen, S. Lebegue, J. Paier, O. A. Vydrov, and J. G. Ángyán, Phys. Rev. B **79**, 155107 (2009).
[59] V. L. Moruzzi, J. F. Janak, and K. Schwarz, Phys. Rev. B **37**, 790 (1988).
[60] P. Mohn (private communication).
[61] H. Kobayashi, J. Umemura, X.-W. Zhang, and Y. Uwatoko, J. Phys.: Conf. Ser. **121**, 032009 (2008).
[62] S. Kumar, A. Krishnamurthy, B. K. Srivastava, and S. K. Paranjpe, J. Phys.: Condens. Matter **19**, 196217 (2007).
[63] A. Koumina, M. Bacmann, D. Fruchart, J.-L. Soubeyroux, P. Wolfers, J. Tobola, S. Kaprzyk, S. Niziol, M. Mesnaoui, and R. Zach, Ann. Chim. Sci. Mat. **23**, 177 (1998); A. Koumina, M. Bacmann, D. Fruchart, M. Mesnaoui, and P. Wolfers, Moroccan Journal of Condensed Matter **5**, 117 (2004).
[64] X. B. Liu and Z. Altounian, J. Appl. Phys. **105**, 07A902 (2009).
[65] P. Söderlind, L. Nordström, Lou Yongming, and B. Johansson, Phys. Rev. B **42**, 4544 (1990).
[66] O. Beckman, L. Lundgren, P. Nordblad, P. Svedlindh, A. Törne, Y. Anderson, and S. Rundqvist, Phys. Scr. **25**, 679 (1982).
[67] G. Grimvall, *Thermophysical Properties of Materials*, revised edition (North-Holland, Amsterdam, 1999).
[68] P. Mohn, *Magnetism in the Solid State* (Springer, Berlin, 2006).
[69] Y. Takahashi, J. Phys.: Condens. Matter **2**, 8405 (1990).
[70] A. Z. Solontsov and D. Wagner, Phys. Rev. B **51**, 12410 (1995).
[71] A. Solontsov and A. Mirmelstein, Phys. Lett. A **372**, 2086 (2008).
[72] A. Z. Solontsov, V. K. Orlov, S. A. Kiselev, and A. A. Burmistrov, At. Energy **107**, 263 (2009).
[73] H. Fujii, Y. Uwatoko, K. Motoya, Y. Ito, and T. Okamoto, J. Phys. Soc. Jpn. **57**, 2143 (1988).
[74] P. Söderlind, O. Eriksson, B. Johansson, J. M. Wills, and A. M. Boring, Nature (London) **374**, 524 (1995).
[75] H. L. Skriver, Phys. Rev. B **31**, 1909 (1985).
[76] G. Grimvall, Phys. Rev. B **39**, 12300 (1989).
[77] G. Grimvall, Phys. Scr. **13**, 59 (1976).